processes

MDPI

Article

Re-Calibrating the Mercury-Intrusion-Porosimetry-Measured Pore Size Distribution of Coals: A Novel Method for Calculating the Matrix Compression Coefficient

Bin Ren [1,2,3], Sijian Zheng [1,2,*], Lihua Ping [4,5], Meng Wang [1,2,*], Xuguang Dai [1,2], Yanzhi Liu [1,2], Shen Xu [1,2] and Xiuping Wu [4,5]

1 Jiangsu Key Laboratory of Coal-Based Greenhouse Gas Control and Utilization, China University of Mining and Technology, Xuzhou 221108, China; ts22010058a31@cumt.edu.cn (B.R.); 18252430765@163.com (X.D.); ts23820005a31@cumt.edu.cn (Y.L.); ts22010157p31@cumt.edu.cn (S.X.)
2 Carbon Neutrality Institute, China University of Mining and Technology, Xuzhou 221008, China
3 School of Resources and Geosciences, China University of Mining and Technology, Xuzhou 221116, China
4 Jiangsu Bureau of Coal Geology, Nanjing 210046, China; 12542363@qq.com (L.P.); 314689318@qq.com (X.W.)
5 China Coal Changjiang Geology Group, Nanjing 210046, China
* Correspondence: sijian.zheng@cumt.edu.cn (S.Z.); wangm@cumt.edu.cn (M.W.)

Abstract: Accurate measurement of the pore size distribution (PSD) in coals is crucial for guiding subsequent coalbed methane (CBM) engineering practice. Currently, mercury intrusion porosimetry (MIP) measurement has been widely used as a PSD testing method due to its effectiveness and convenience. Nevertheless, it is worth noting that the elevated pressure during the MIP experiments can lead to matrix compressibility, potentially causing inaccurate estimations of PSD in coals. Therefore, correction methods are used to modify the PSD in the high-pressure segment to improve the accuracy of MIP data. This study proposed a novel method with higher accuracy and convenience for calculating the matrix compressibility coefficient compared to the traditional calculation methods. Firstly, the matrix compressibility coefficients of six coal samples were calculated by using low-temperature nitrogen adsorption (LTNA) data. Subsequently, by utilizing the mathematical correlation between K_c (the compressibility coefficient of the coal matrix) and $R_{o,max}$ (the maximum vitrinite reflectance) from prior research, a novel statistical method was designed to determine the matrix compressibility coefficient of the samples. Finally, the statistical matrix compressibility coefficient determination method was used to examine the fractal characteristics of the actual PSD. The results indicate that when the pressure exceeds 24 MPa, the volume obtained from mercury intrusion exceeds the pore volume measurement. The K_c calculated using the traditional correction method is in the range of 0.876–1.184 $\times 10^{-10}$ m^2/N, while the K_c values of our proposed statistical correction method range from 0.898 $\times 10^{-10}$ to 1.233 $\times 10^{-10}$ m^2/N, with a comparison error rate of ~0.11–5.25%. The MIP data greater than 24 MPa were effectively corrected using the statistical correction method, thus reducing the mercury intrusion volume error by 91.75–96.40%. Additionally, the corrected pore fractal dimension (D_2) values fall within the range of 2.792 to 2.975, which are closer to the actual values than the pore fractal dimension range of 3.186 to 3.339.

Keywords: coal matrix compression effect; mercury intrusion method (MIP); pore size distribution (PSD); fractal dimension; correction method

Citation: Ren, B.; Zheng, S.; Ping, L.; Wang, M.; Dai, X.; Liu, Y.; Xu, S.; Wu, X. Re-Calibrating the Mercury-Intrusion-Porosimetry-Measured Pore Size Distribution of Coals: A Novel Method for Calculating the Matrix Compression Coefficient. *Processes* **2024**, *12*, 1928. https://doi.org/10.3390/pr12091928

Academic Editors: Ye Huang and Raymond Cecil Everson

Received: 4 August 2024
Revised: 28 August 2024
Accepted: 5 September 2024
Published: 8 September 2024

1. Introduction

The commercial production of coalbed methane (CBM) truly began after the 1970s. The United States was one of the first countries to commercialize CBM production, experiencing a progression from experimental stages to large-scale commercialization, with its CBM production rapidly increasing, making it a global leader in bed methane development. Other countries, such as Australia, China, and Canada, have also started large-scale development of CBM resources. Currently, the global CBM industry has reached a particular

scale, becoming an essential supplement to the natural gas supply [1]. During the extraction of CBM, the pore size distribution (PSD) of coal reservoirs and their variations are vital for the permeation and retention of CBM [2–5]. Therefore, accurately characterizing the PSD is crucial for improving energy development efficiency. Understanding the PSD helps optimize extraction methods, improve gas recovery rates, and ensure the efficient utilization of coalbed methane resources.

Existing methods for characterizing coal PSD include both direct and indirect approaches [6–11]. Low-temperature gas adsorption measurements are only suitable for testing the PSD characteristics of smaller apertures [12–14]. Some image-testing techniques (e.g., scanning electron microscope and transmission electron microscope) can visually observe the exterior of pores through image processing, but the PSD data obtained are not representative [15,16]. MIP is a physical, analytical technique employed for the assessment of the pore structure within various materials. This technique measures parameters, such as pore size and distribution, by applying high pressure to force mercury into the material's pores, and it is considered an important method for analyzing PSD [17–21].

Because of the coal matrix's high compressibility [22–25], excessive pressure within the pores can cause the coal matrix to deform or even fracture. This deformation may lead to the mercury intrusion volume surpassing the actual pore volume. This inevitably affects the accuracy of the fractal dimension calculation for the coal PSD. Therefore, when using MIP and fractal dimensions to characterize PSD, it is imperative to comprehensively account for the compressive effects of the coal matrix and implement suitable correction measures to guarantee the precision and validity of the measurement results.

Previous studies have demonstrated that various factors influence the measured pore volumes in coals during MIP experiments. At medium- to high-pressure stages, the pore-filling mechanism and matrix-shrinkage effect directly controlled the determined PSD and other pore parameters [26]. Some researchers have determined the relationship between mercury intrusion pressure and coal deformation in a specific pressure range, using relevant methods to calculate the matrix compression coefficient in coals [27,28]. It has been recognized that the coal matrix compression effect becomes significant when the mercury intrusion pressure exceeds 10 MPa [29]. Jin et al. [30] analyzed the changing pattern of coal matrix pore characteristics with pressure based on coal matrix compressibility. After that, the complexity of pore structures was concisely described by using fractal theory. Liu et al. [31] considered the matrix-compression effect and analyzed its impact on pores of different size ranges. Han et al. [32] found that coal samples exhibit significant compressibility during MIP tests and that the pore volume decreases with increasing pressure. Zheng et al. [33] calculated the coal matrix compression coefficient and characterized its PSD by correcting it with fractal theory.

The degree of coal metamorphism is a significant factor affecting the compressibility of the coal matrix. The study by Guo et al. [34] indicates that when $R_{o,max}$ (maximum vitrinite reflectance) is between 0.65 and 0.99%, the compressibility of the coal matrix shows a rapid decline. In contrast, when $R_{o,max}$ is between 1.25 and 1.77%, the compressibility shows an increasing trend. Similarly, Ettinger and Zhupakhina's [35] research also observed this trend and described it as a U-shaped relationship curve. Zheng et al. [33] found that as the degree of metamorphism evolves from medium to high, the compressibility of the coal matrix increases, and the vitrinite and inertinite groups have opposite effects on the compressibility of the coal matrix. Lu's [36] research indicates that the coal matrix compressibility coefficient exhibits a three-stage change trend with the increase of $R_{o,max}$.

In summary, in previous studies on MIP data correction, traditional correction methods require extensive preparation, involve substantial calculations, and rely heavily on test data obtained through LTNA experiments. Without conducting LTNA experiments, MIP data correction cannot be performed. When assessing the impact of coal matrix compressibility on the permeability and porosity of coalbed methane reservoirs, such traditional correction methods result in low MIP data correction efficiency, higher experimental costs, and increased complexity. On the other hand, more studies have shown the relationship

between the coal matrix compressibility coefficient (*Kc*) and the increase in $R_{o,max}$, but they have yet to consider utilizing this trend to calculate the coal matrix compressibility coefficient (*Kc*).

In response to the issues in previous MIP data correction studies, this research proposes a new MIP data correction method (the statistical correction method). The method is based on the coal matrix compressibility coefficient (*Kc*) and $R_{o,max}$ values calculated in previous studies [9,17,33,37–43], fitting their mathematical relationship to calculate the matrix compressibility coefficient of coal samples and correcting the MIP data exceeding 24 MPa. This study further investigates the changes in pore fractal dimensions before and after correction, indirectly validating the accuracy of the proposed method. This method successfully depicts the three-stage variation trend of the matrix compressibility coefficient of coal samples with different degrees of metal as the maximum vitrinite reflectance increases, making it possible to determine the matrix compressibility coefficient based solely on the maximum vitrinite reflectance of coal samples. Therefore, this method simplifies the correction process during MIP data correction, eliminating the need for specialized low-temperature nitrogen adsorption (LTNA) experiments. Compared with traditional correction methods (based on LTNA data), this method significantly reduces experimental preparation and the computational workload, facilitating a deeper understanding and revealing the characteristics of coal pore size distribution, thus making it more practical. Introducing this method helps optimize the complex process of CBM reservoir evaluation, thereby enhancing its applicability.

2. Samples and Experiments

The Qinshui Basin, located in northern China, is rich in coal resources and contains abundant natural gas and coalbed methane resources [44–50]. Significant progress has been made in developing CBM in this region in recent years. This experiment collected coal samples from six distinct mining areas (DD, QX, TL-2, TL-8, WK, and YY) within the southern Qinshui Basin. Among them, the DD and QX mines are located in the Zhengzhuang block, the TL-2 and TL-8 mines are in the Mabi block, and the WK and YY mines are in the Fanzhuang block (Figure 1). Samples were extracted from the working faces of underground mines to ensure freshness and integrity. The coal samples were wrapped in absorbent paper, sealed with adhesive tape, and placed in sealed bags before being promptly transported to the laboratory for MIP, LTNA, and maximum vitrinite reflectance testing.

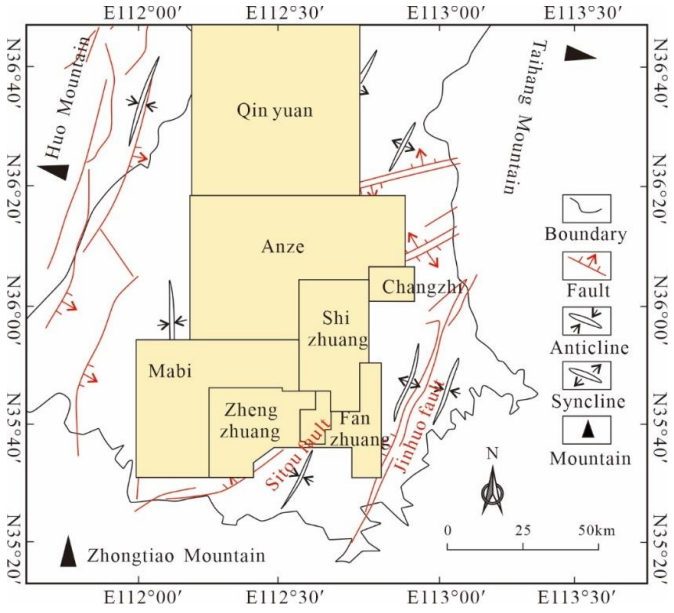

Figure 1. Structural outline map of the southern Qinshui Basin.

The MIP measurements were performed using a Micromeritics Autopore 9510 instrument of the standard SY/T5346-2005 [51]. The sample dimensions were approximated in ~2 mm length, width, and height (Figure 2).

The LTNA test was performed using an Autosorb iQ (Quantachrome, FL, USA). After grinding, the coal powder was sieved with a 40–60 mesh sieve and dried in a vacuum oven at a constant temperature for 24 h before testing.

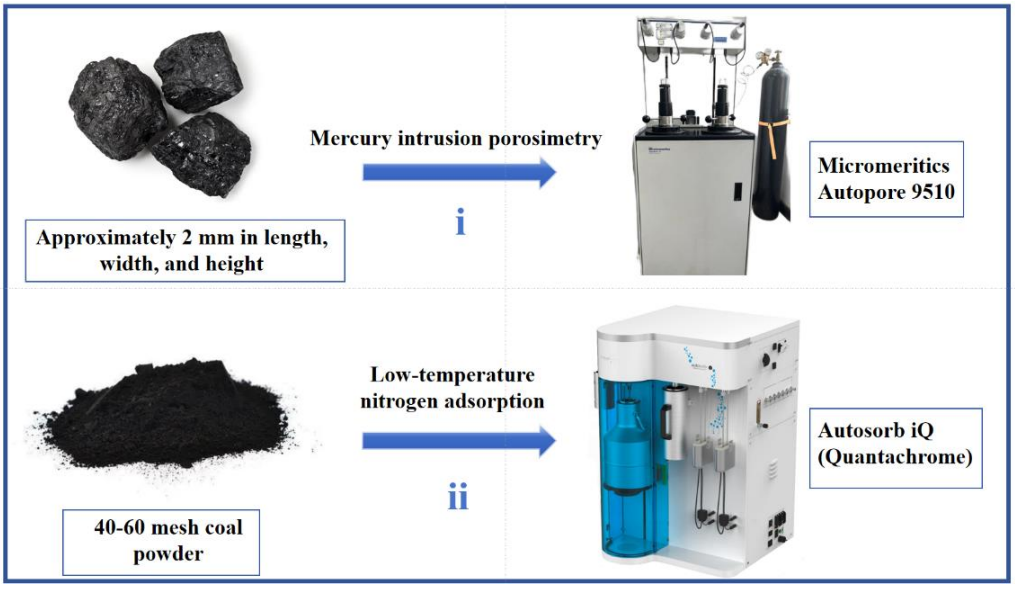

Figure 2. Experimental samples and equipment.

3. Results and Discussion

3.1. MIP Experimental Results

Various MIP experimental parameters offer insights into pore connectivity, development, and coal matrix compressibility from multiple perspectives. By analyzing MIP data from samples collected across different mining areas, mercury intrusion and extrusion curves, along with the PSDs, were obtained. The MIP curves of coal samples from six distinct mining areas could be categorized into three types (Figure 3). Type I (Samples DD and QX): the mercury intrusion and extrusion curves exhibit similar slopes with no significant hysteresis loop, indicating predominantly semi-open pores with poor connectivity, which is not conducive to gas flow. Type II (Samples TL-8, WK, and YY): the mercury intrusion and extrusion curves have similar slopes at high pressures but demonstrate hysteresis at low pressures, suggesting poor connectivity in the transitional pores segment and better connectivity in the more significant pore segment. Type III (Sample TL-2): the curve indicates that as the pressure increases, the mercury intrusion volume significantly rises at lower pressures, with a wide curve opening and evident hysteresis, indicating predominantly open pores with good connectivity, which is not favorable for gas storage. Notably, as the mercury intrusion pressure increases, all selected samples in this article show a significant increase trend in the cumulative mercury intrusion volume when the pressure exceeds ~10 MPa because of the coal matrix compressibility. Failure to account for this effect during data analysis may result in overestimating the number of micropores.

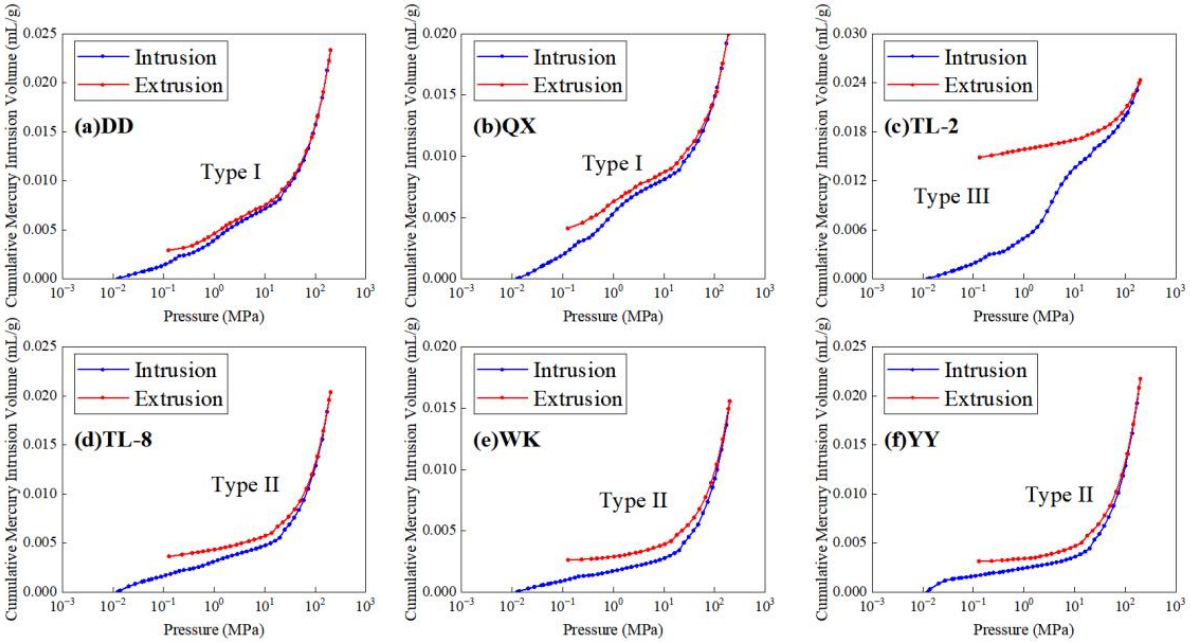

Figure 3. Mercury intrusion and extrusion curves of six selected coals. (Type I (Samples DD and QX): the mercury intrusion and extrusion curves exhibit similar slopes with no significant hysteresis loop, indicating predominantly semi-open pores with poor connectivity, which is not conducive to gas flow. Type II (Samples TL-8, WK, and YY): the mercury intrusion and extrusion curves have similar slopes at high pressures but demonstrate hysteresis at low pressures, suggesting poor connectivity in the transitional pores segment and better connectivity in the more significant pore segment. Type III (Sample TL-2): the curve indicates that as the pressure increases, the mercury intrusion volume significantly rises at lower pressures, with a wide curve opening and evident hysteresis, indicating predominantly open pores with good connectivity, which is not favorable for gas storage).

3.2. LTNA Experimental Results

LTNA curves are commonly used to characterize pore structures by analyzing the hysteresis loops generated during adsorption and desorption. Examining different types of adsorption–desorption curves allows for identifying various pore characteristics. Through horizontal comparison of different coal experimental data with the IUPAC classification of hysteresis loops, the experimental curves could be categorized into three types (Figure 4).

Type I curves (Samples No. DD, WK, and YY) exhibit significant adsorption–desorption hysteresis loops within the P/P0 range of 0.4–1, characterized by a sharp drop, indicating the existence of bottleneck breakthroughs and ink-bottle-shaped pores. Type II curves (Sample No. QX) display nearly parallel adsorption and desorption curves with indistinct hysteresis loops, signifying half-open, plate-like pores. Type III curves (Samples No. TL-2 and TL-8) resemble Type II curves but exhibit more distinct hysteresis loops in the P/P0 range of 0.7–1, which indicates the presence of open plate-like pores. Ink-well-bottle pores and half-open, plate-shaped pores are conducive to the adsorption of coalbed methane. However, they are unfavorable for its desorption, making it difficult for coalbed methane to migrate to seepage channels and coalbed methane wells quickly. In contrast, due to their simple pore structure, open plate-shaped pores are more favorable for the desorption and migration of coalbed methane.

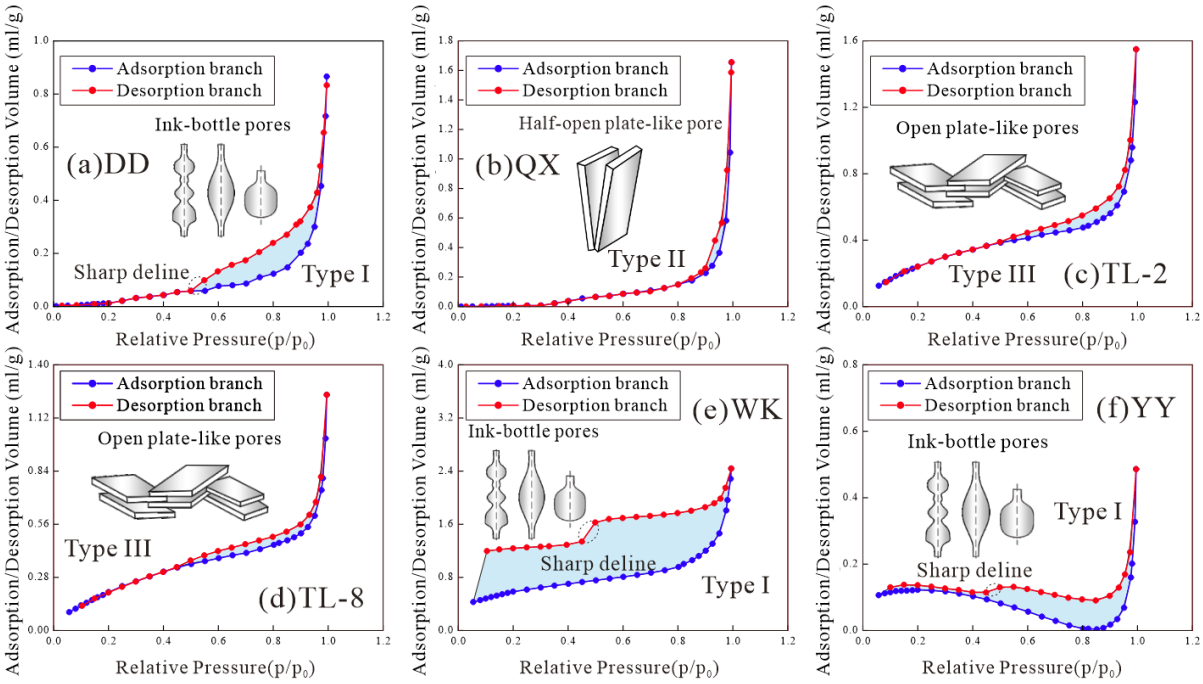

Figure 4. Adsorption–desorption curves of six selected coals. (Type I curves (Samples No. DD, WK, and YY) exhibit significant adsorption–desorption hysteresis loops within the P/P0 range of 0.4–1, characterized by a sharp drop, indicating the existence of bottleneck breakthroughs and ink-bottle-shaped pores. Type II curves (Sample No. QX) display nearly parallel adsorption and desorption curves with indistinct hysteresis loops, signifying half-open, plate-like pores. Type III curves (Samples No. TL-2 and TL-8) resemble Type II curves but exhibit more distinct hysteresis loops in the P/P0 range of 0.7–1, which indicates the presence of open plate-like pores).

3.3. Considering MIP Data Correction for Matrix Compression

3.3.1. Traditional Correction Method

An analysis of MIP experimental data from six coal samples from various mining regions reveals that when mercury injection pressure surpasses 24 MPa, a strong linear relationship exists between the cumulative mercury injection volume and the injection pressure, with correlation coefficients exceeding 0.99 (Figure 5). This indicates a remarkable compression effect on the coal matrix at pressures above 24 MPa. Assuming the mercury compressibility and instrument are negligible, the coal matrix compression effect can be described as follows [52]:

$$K_c = \frac{dV_c}{V_c dP_c} \quad (1)$$

where K_c represents the matrix compression coefficient, 10^{-10} m^2/N; V_c represents the coal matrix volume, and cm^3/g; dV_c represents the coal matrix volume increment at a pressure of dP_c, cm^3/g.

Research indicates that when the mercury intrusion pressure exceeds 20 MPa, the compression effect on the coal matrix becomes significant [53–56]. At this stage, the variation in the mercury injection volume of the coal sample is attributed to the combined effects of pore filling and matrix compression [52].

$$\Delta V_d = \Delta V_p + \Delta V_c \quad (2)$$

where ΔV_d represents the mercury intrusion volume; ΔV_p denotes the pore-filling volume; and ΔV_c is the change in the volume of matrix compression, all measured in cm^3/g.

Combining MIP test data with LTNA test data, the appropriate correction range is 24 MPa–200 MPa (the corresponding pore size range is 3–25 nm). Before the correction, the

volume and pressure of mercury intrusion within the correction range of the coal sample exhibit a linear relationship. Therefore, $\Delta V_d/\Delta P$ is considered a constant C, resulting in $\Delta V_c/\Delta P$ [52]:

$$\frac{\Delta V_c}{\Delta P} \approx C - \frac{\sum_{3nm}^{25nm} \Delta V_p}{\Delta P} \quad (3)$$

where ΔP represents the pressure increment in MPa and ΔV_p represents the pore volume within the 3–25 nm range obtained from LTNA test data, in mL/g.

Because $\Delta V_c/\Delta P$ can be approximated as a constant, using $\Delta V_c/\Delta P$ instead of dV_c/dP_c, the K_C can be obtained by combining Equations (1) and (3).

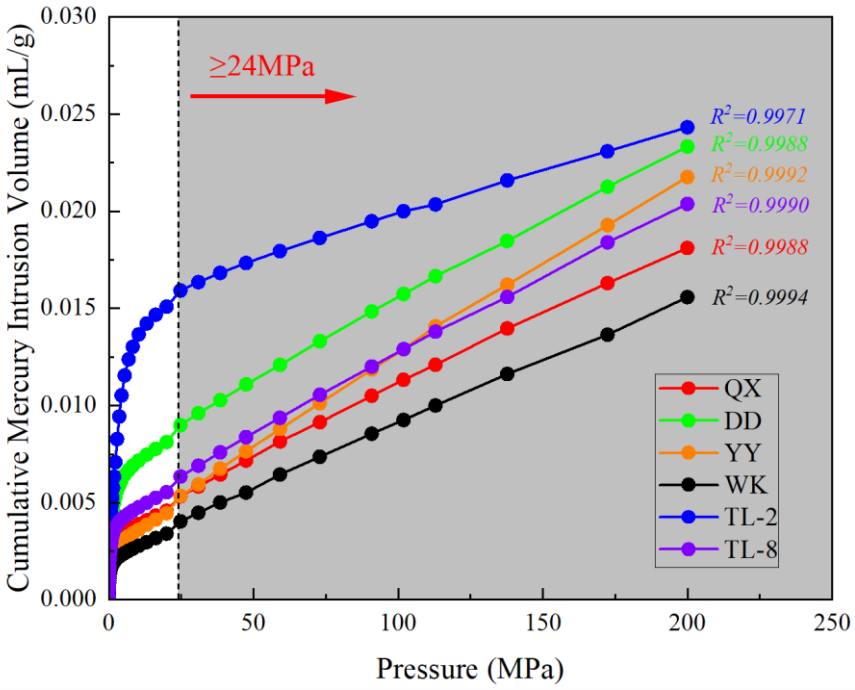

Figure 5. Linear variation of mercury intrusion volume with pressure for coal samples.

3.3.2. Statistical Correction Method

The traditional correction method corrects MIP data through LTNA data, but explicitly testing LTNA data to achieve the purpose of correcting MIP data has the disadvantages of high cost, a long time, and low efficiency, with certain limitations. In response, a statistical correction method for MIP data correction is proposed. The specific method is as follows. Based on the statistical analysis of K_C data from 176 different coal samples, the samples are divided into three groups according to their degrees of metamorphism: low metamorphism ($0.35\% \leq R_{o,max} < 0.65\%$), medium metamorphism ($0.65\% \leq R_{o,max} \leq 2.00\%$), and high metamorphism ($R_{o,max} > 2.00\%$). For each group, the K_C data are averaged based on $R_{o,max}$ intervals of 0.05%, and this method is used to fit the relationship between K_C and $R_{o,max}$ for coal samples of different metamorphic degrees. First, different coal samples' matrix compressibility coefficients (K_C) are calculated using the fitting Equation (4). Then, based on the obtained K_C values, Equation (5) is applied to calculate the matrix compressibility volume for each sample. Finally, Equation (6) is used to subtract the incremental mercury intrusion volume from the original MIP data to obtain the corrected actual pore volume increment, thus completing the correction of the MIP data. Figure 6 shows the trend of K_C increasing with $R_{o,max}$ with a low metamorphism degree ($0.35\% \leq R_{o,max} < 0.65\%$), decreasing with a medium metamorphism degree ($0.65\% \leq R_{o,max} \leq 2.00\%$), and increasing with a high metamorphism degree ($R_{o,max} > 2.00\%$). The K_C calculation formula is obtained through a fitting analysis of the data with different metamorphism degrees:

$$K_c = \begin{cases} 91.509R_{o,max}^3 - 144.07R_{o,max}^2 + 77.029R_{o,max} - 10.791 \ (0.35\% \le Ro, max < 0.65\%) \\ -1.5392R_{o,max}^3 + 6.8265R_{o,max}^2 - 11.108R_{o,max} + 7.8239 \ (0.65\% \le Ro, max \le 2.00\%) \\ -2.3236R_{o,max}^3 + 17.964R_{o,max}^2 - 45.084R_{o,max} + 37.674 \ (Ro, max > 2.00\%) \end{cases} \quad (4)$$

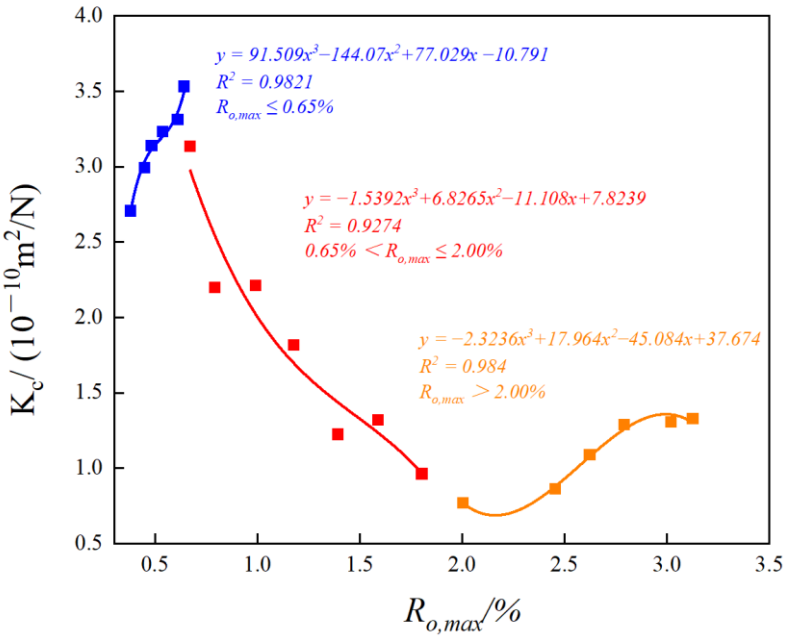

Figure 6. The fitted curve of K_C with varying $R_{o,max}$.

The formula's fitting degrees for different metamorphic grades are 0.9821, 0.9274, and 0.984, respectively, demonstrating the formula's strong capability to represent the K_C value accurately.

Using the traditional correction method, the K_{C1} value was calculated through MIP test data and LTNA test data in conjunction with Formulas (1) and (3). Simultaneously, using the proposed method, the K_{C2} value was calculated by combining the $R_{o,max}$ values of different collected samples with Formula (4). Figure 7 visually demonstrates the comparison of K_C values calculated using the two methods.

Table 1 presents the $R_{o,max}$ for six selected coals from six mining regions alongside the K_{C1} values determined through the traditional correction method and the K_{C2} values calculated using the statistical correction method, which are consistent with previous research results of 0.67×10^{-10} m^2/N–3.06×10^{-10} m^2/N [57,58], proving the rationality of Formula (4). It can be seen that the error rate range between K_{C1} and K_{C2} is 0.11–5.25%, indicating that the K_C values calculated using the statistical correction method have good accuracy and reliability. From this, it can be seen that the statistical correction method proposed in this study has the following advantages over traditional correction methods: when calculating the coal matrix compression coefficient K_C, only the maximum vitrinite reflectance parameter is needed. This significantly reduces experimental preparation and the computational workload, simplifies the MIP data correction process, and avoids the traditional method's over-reliance on LTNA test data for correcting MIP data. It is particularly noted that within the high metamorphism range ($R_{o,max}$ > 2.00%), the K_{C1} value calculated using this method has minimal error compared to the value calculated using traditional methods, and it is very close to the actual value (K_{C2}). In the preliminary evaluation stage of the compressibility of coal in coalbed methane reservoirs, using the method proposed in this study dramatically improves the evaluation efficiency (it only requires substituting the maximum vitrinite reflectance into Formula (4) for evaluation), and it can directly serve as a reference.

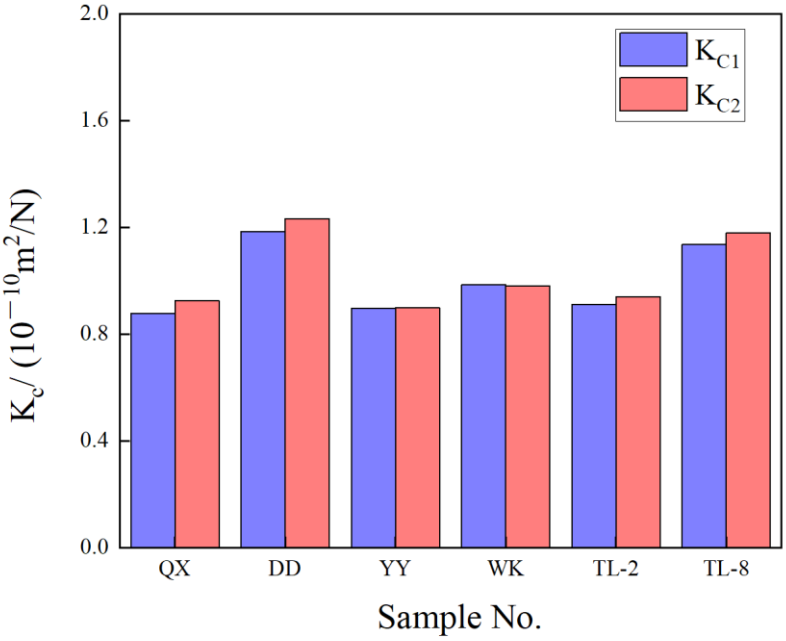

Figure 7. Comparison of traditional correction method K_{C1} and statistical correction method K_{C2}.

Table 1. $R_{o,max}$ values and coal matrix compression coefficients for different coal samples.

Sample No.	$R_{o,max}$/%	K_c/(10^{-10} m^2/N)		Error Rate
		K_{c1}	K_{c2}	
QX	1.83	0.876	0.925	5.25%
DD	1.59	1.184	1.233	3.97%
YY	2.47	0.897	0.898	0.11%
WK	2.54	0.984	0.980	0.35%
TL-2	1.82	0.911	0.940	3.12%
TL-8	1.64	1.137	1.178	3.50%

3.4. Analysis of Calibration Results

Research indicates that during the mercury intrusion process, when the compressibility coefficient of the coal matrix is considered a constant, the volume of the coal sample can be corrected using Formula (5) [52]:

$$V_{c(P_i)} = V_c - \frac{dV_c}{dP_c}(P_i - P_0) \quad (5)$$

where $V_{c(Pi)}$ represents the volume of the coal matrix under pressure P_i, measured in cm^3/g; r denotes the serial number of the pressure collection point; and P_0 is set to 24 MPa.

The pore-filling volume of the coal sample under pressure P_i can be calculated using Equation (6) [52]:

$$\Delta V_{pi} = \Delta V_d - K_c V_{c(P_i)}(P_i - P_0) \quad (6)$$

where ΔV_{pi} represents the volume change of the coal matrix at the mercury intrusion pressure P_i, cm^3/g; ΔV_d represents the mercury intrusion volumes at the pressures P_i and P_0, respectively, in cm^3/g; and K_C is the K_{C2} calculated using the statistical correction method (see Table 1), 10^{-10} m^2/N.

By integrating Equations (5) and (6), this study calculated the coal's cumulative mercury intrusion volumes before and after correction. As shown in Figure 8, the data reveal a significant discrepancy in cumulative mercury intrusion volumes before and after correction. The theoretical analysis results suggested that the corrected MIP data show substantial improvement, thus facilitating a more accurate characterization of the coal

samples' pore structure. The PSD of the coals determines their pore structure characteristics. According to Hodot's (1966) pore-classification methodology, pores are categorized into micropores (<10 nm), transitional pores (10–100 nm), mesopores (100–1000 nm), and macropores (>1000 nm).

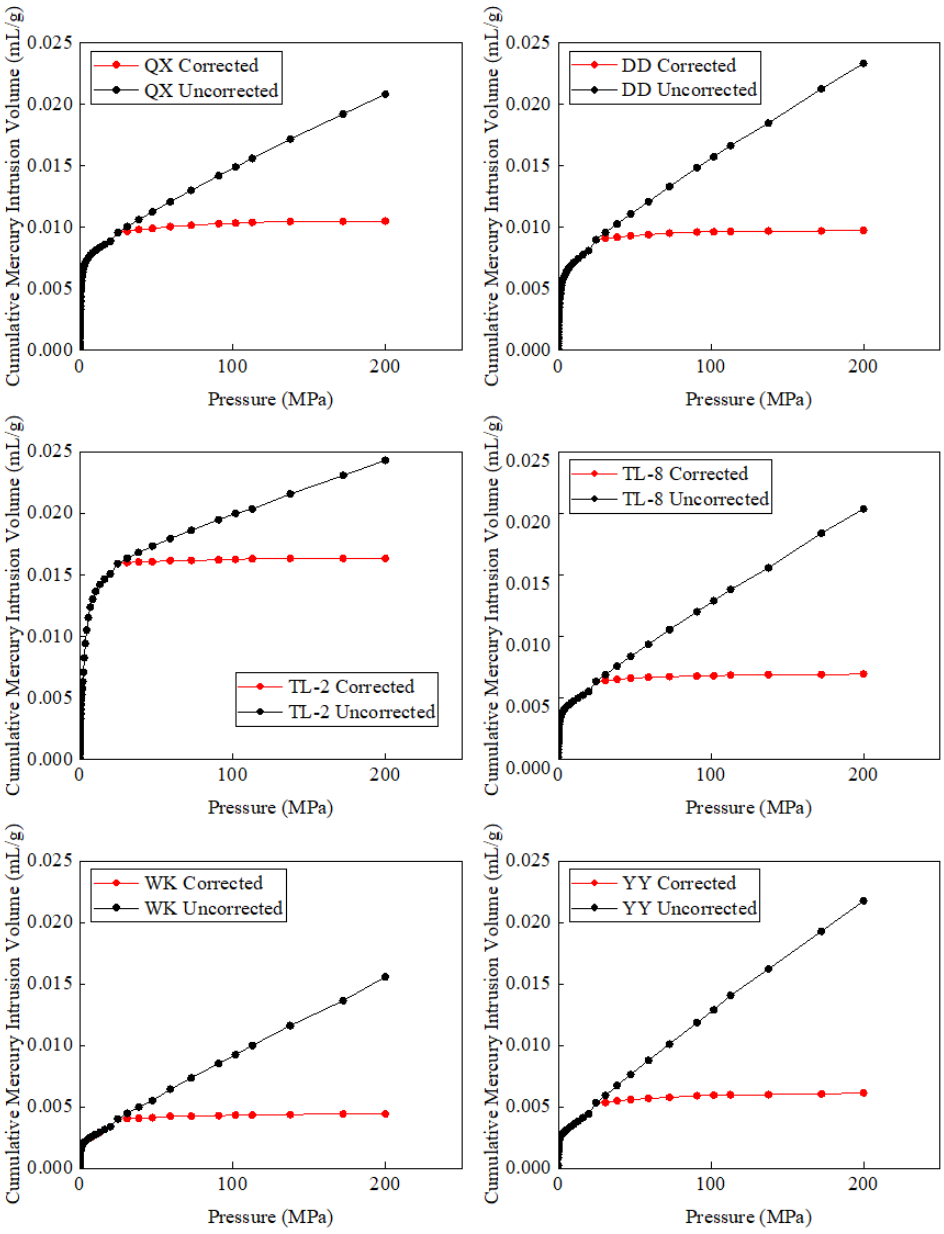

Figure 8. Cumulative volume of mercury ingress before and after calibration.

Figure 9 presents the PSD and the volume proportions of various pores in the corrected coal samples. The pore structure of the coal samples predominantly comprises macropores, followed by mesopores and transitional pores, with micropores constituting the most minor proportion. Compared to the mercury intrusion volumes before correction, the 3–25 nm pore radius range decreases the mercury intrusion volume by 91.75–96.40% after correction, indicating a successful correction effect. This implies that the coal matrix's compressibility significantly impacts the PSD measurement in MIP experiments.

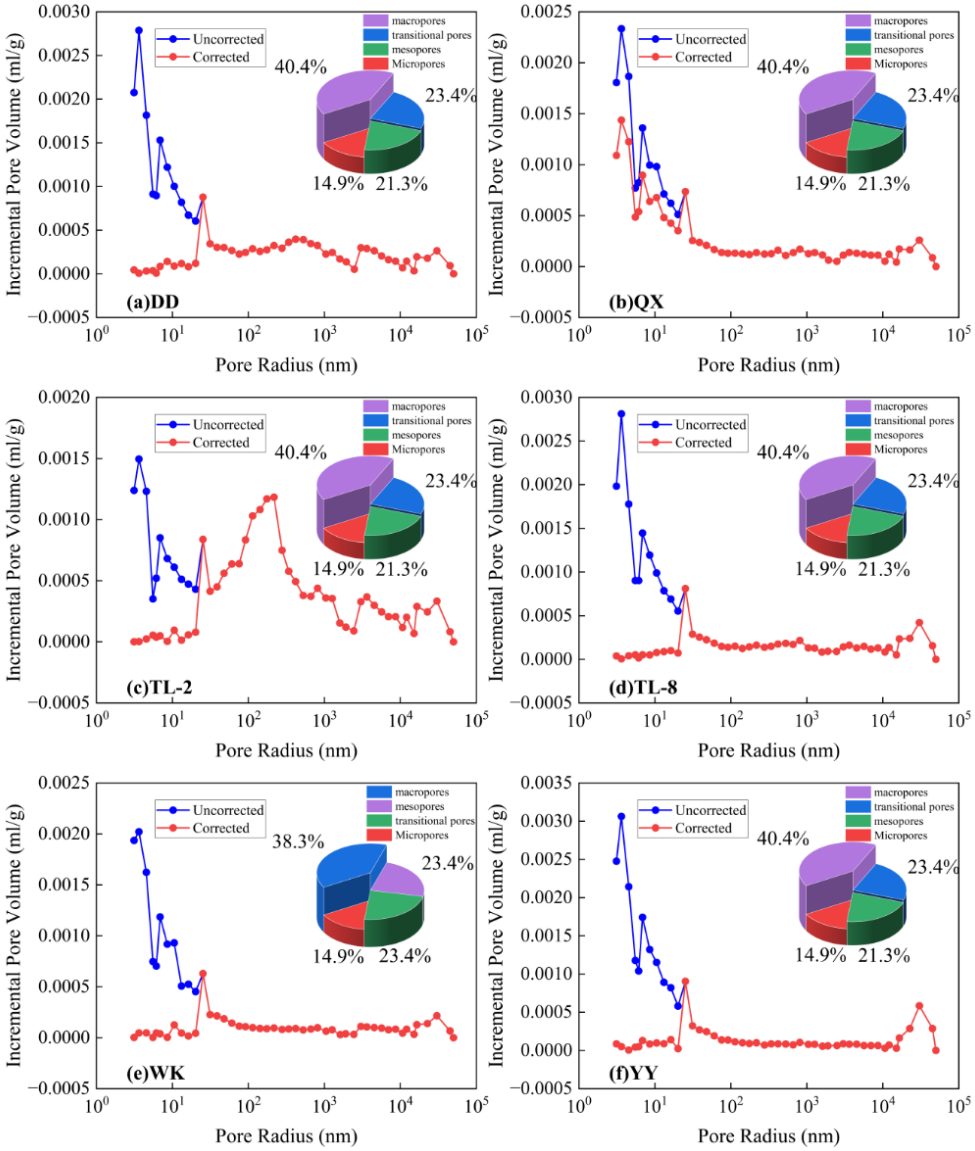

Figure 9. The correction results of PSD and the aperture ratio. (The pore structure of the coal samples predominantly comprises macropores, followed by mesopores and transitional pores, with micropores constituting the most minor proportion. Compared to the mercury intrusion volumes before correction, the 3–25 nm pore radius range decreases the mercury intrusion volume by 91.75–96.40% after correction).

4. Fractal Dimension Characteristics before and after Calibration

The MIP pore structure exhibits fractal characteristics, which can be used to illustrate the influence of pre- and post-correction of MIP data on the fractal properties of the pores using fractal geometry concepts, thereby characterizing the pore morphology of coal. The Menger sponge model, a universal fractal calculation curve with a topological dimension of 1 [59], has been extensively applied to porous media. After repeated verification by scholars, it has ultimately been simplified into a general model:

$$D_2 = 4 + \lg\left(\frac{dV}{dP}\right) / \lg P \tag{7}$$

where P represents the pressure during the mercury intrusion process, measured in MPa; V represents the incremental volume of mercury intrusion in the interval, measured in mL/g; and D_2 denotes the pore fractal dimension, which is dimensionless.

Figure 10 compares the fractal dimension D_2, calculated from MIP data within the pressure range of 24 MPa to 200 MPa, before and after correction. The corrected fractal dimension D_2 shows a substantial improvement over the uncorrected values. Figure 11 shows that before correction, the D_2 values range from 3.186 to 3.339, indicating fractal dimensions between 3 and 4, which suggests suboptimal fractal characteristics of the overall pore structure. At this stage, the filling effect coexists with the matrix compression effect, with the latter predominating. This predominance results in significant measurement deviations, hindering an accurate reflection of the true pore structure.

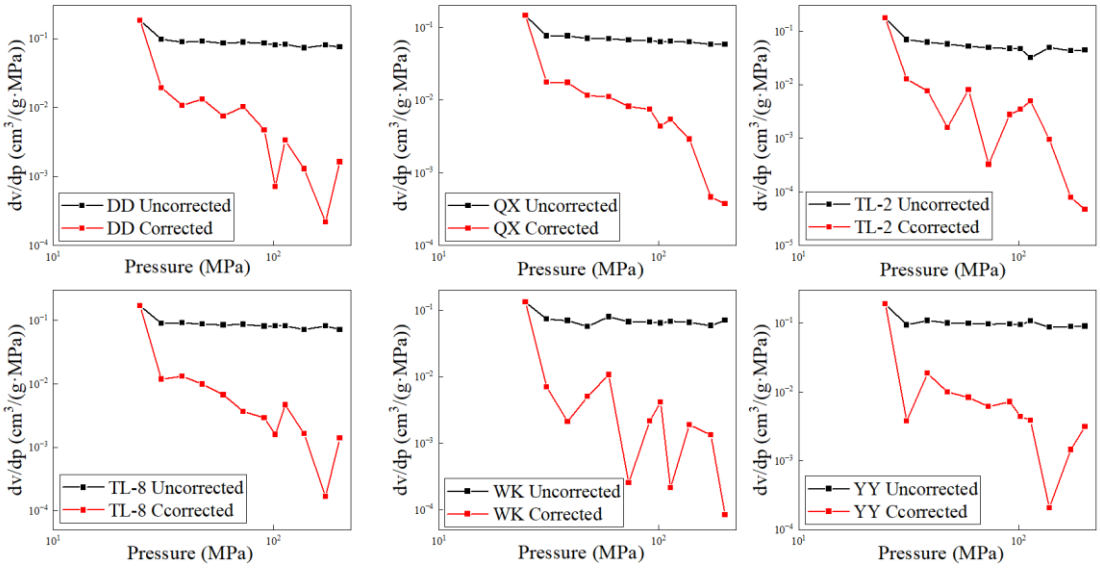

Figure 10. The changes in fractal dimension D_2 before and after MIP data correction.

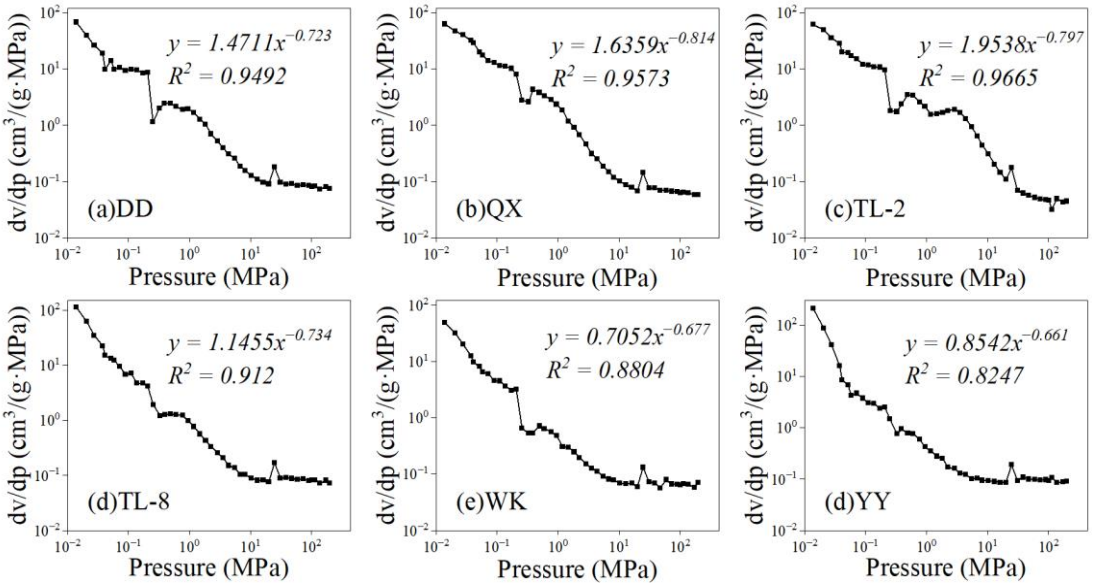

Figure 11. The correlation between pressure and dV/dP before MIP data adjustment. (The D_2 values range from 3.186 to 3.339, indicating fractal dimensions between 3 and 4).

Figure 12 illustrates the relationship between pressure and dV/dP for the six groups of corrected coal samples. The figure shows that the adjusted fractal dimension D_2 ranges from 2.792 to 2.975 within the expected range of 2 to 3, demonstrating robust fractal characteristics. This indicates that the correction process is highly effective, providing a more accurate and reliable depiction of the pore structure. The corrected fractal dimension values show that the pore sizes of the six coal samples collected in this study are well-developed

at all stages. Compared to mesopores and macropores, the surfaces of micropores and transitional pores are rougher. The pore size distribution is complex, with irregular shapes and firm heterogeneity, making it easier to store free gas.

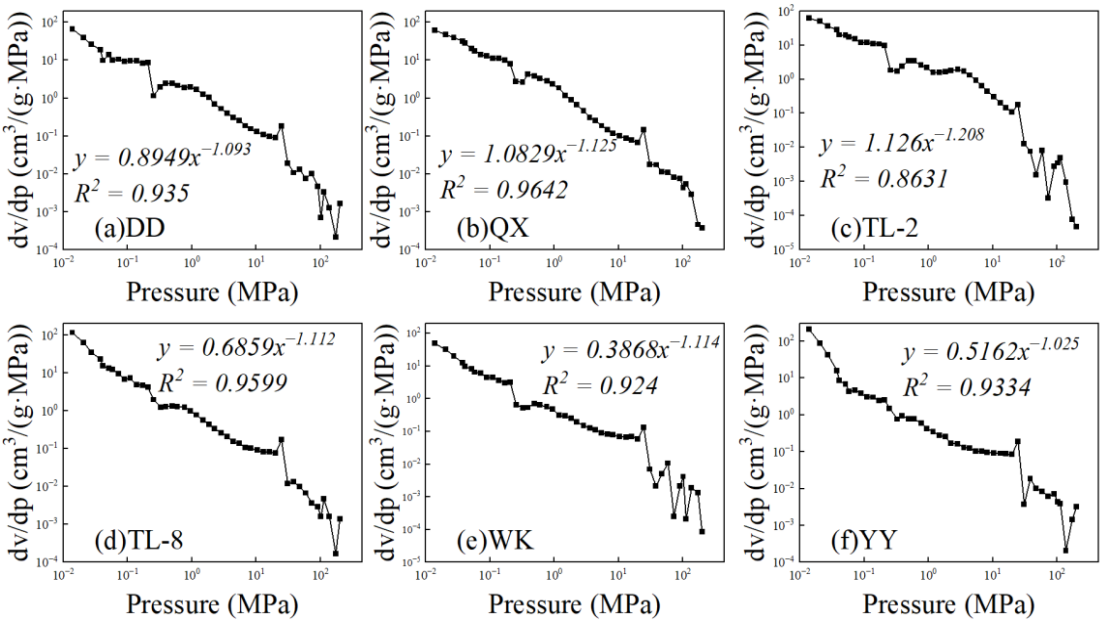

Figure 12. The correlation between pressure and dV/dP after MIP data correction. (The adjusted fractal dimension D_2 ranges from 2.792 to 2.975 within the expected range of 2 to 3).

5. Research and Prospects

This study innovatively proposes a method for calculating the coal matrix compressibility coefficient based on maximum vitrinite reflectance. However, a specific deviation exists between the empirical formula derived from data statistics and the actual calculated values. On the other hand, as the coal samples used in this study do not belong to the low metamorphic degree ($0.35\% \leq R_{o,max} < 0.65\%$), no error comparison was conducted for K_C value calculation at a low metamorphic degree. Therefore, with the enrichment of research data on K_C and $R_{o,\ max}$ in the industry, future studies using this method should incorporate the calculation of the compressibility coefficient for a low-metamorphic-degree coal matrix and further refine the accuracy of the empirical formula to reduce calculation errors. In the practice of coalbed methane work, the compressibility coefficient of the coal matrix in the reservoir is calculated to evaluate certain parameters, such as permeability and porosity, thereby guiding coalbed methane development.

6. Conclusions

(1) The analysis of MIP data reveals significant differences in the pore structure and the connectivity of coal samples from different mining areas. Type I coal samples predominantly exhibit semi-open pores with poor connectivity. Type II coal samples show poor connectivity in the transitional pores segment but good connectivity in the large pore segment. In contrast, Type III coal samples mainly feature open pores with good connectivity. Furthermore, data from LTNA experiments indicate notable pore morphology variations among coal samples. Ink-bottle, semi-open, and open plate-shaped pores primarily characterize these morphologies.

(2) Considering the matrix compression effect of coal, a novel statistical correction method was devised based on statistical analysis. Compared to K_C values calculated using the traditional correction method, the statistical correction methods have high practical applicability. This statistical correction method was applied to correct MIP data under pressures ranging from 24 to 200 MPa, resulting in a decrease in the corrected mercury

intrusion volume by 91.75% to 96.40%. The correction effect was significant, enabling a more precise characterization of the PSD.

(3) The D_2 of MIP-measured initial uncorrected data values ranged from 3.186 to 3.339, with fractal dimensions between 3 and 4, indicating the suboptimal fractal characteristics of the overall pore structure. After PSD correction, D_2 values ranged from 2.792 to 2.975 within the 2 to 3 range, reflecting improved fractal characteristics. Correcting the MIP data significantly enhances the fractal representation of the coal's pore structure, aligning the fractal dimensions more closely with their true values and thus offering a more accurate depiction.

Author Contributions: Writing—original draft preparation, B.R.; methodology and investigation, S.Z.; software, X.D.; validation, M.W.; formal analysis, Y.L.; resources and data curation, L.P.; visualization, X.W.; supervision, S.X. All authors have read and agreed to the published version of the manuscript.

Funding: This research was funded by the National Natural Science Foundation of China (No. 42302194), the National Key Research and Development Program of China (No. 2023YFE0120500), the Natural Science Foundation of Jiangsu Province, China (No. BK20231084), the Applied Basic Research Programs of Xuzhou, China (No. KC23001), and the Fundamental Research Funds for the Central Universities (No. 2023KYJD1001, 2024KYJD2004).

Data Availability Statement: The raw data supporting the conclusions of this article will be made available by the authors on request.

Conflicts of Interest: Authors Lihua Ping and Xiuping Wu were employed by the company China Coal Changjiang Ge-ology Group. The remaining authors declare that the research was conducted in the absence of any commercial or financial relationships that could be construed as a potential conflict of interest.

References

1. Wang, M.; Xie, W.D.; Huang, K. Fine characterization of lithofacies and pore network structure of continental shale: Case study of the Shuinan Formation in the north Jiaolai Basin, China. *J. Pet. Sci. Eng.* **2019**, *175*, 948–960. [CrossRef]
2. Cai, Y.D.; Liu, D.M.; Pan, Z.J.; Yao, Y.B.; Li, J.Q.; Qiu, Y.K. Pore structure and its impact on CH_4 adsorption capacity and flow capability of bituminous and subbituminous coals from Northeast China. *Fuel* **2013**, *103*, 258–268. [CrossRef]
3. Liu, S.; Harpalani, S. Compressibility of sorptive porous media: Part 1. *Background and theory. AAPG Bull.* **2014**, *98*, 1761–1772. [CrossRef]
4. Zheng, S.J.; Yao, Y.B.; Liu, D.M.; Cai, Y.D.; Liu, Y. Characterizations of full-scale pore size distribution, porosity and permeability of coals: A novel methodology by nuclear magnetic resonance and fractal analysis. *Int. J. Coal Geol.* **2018**, *196*, 148–158. [CrossRef]
5. Moore, T.A. Coalbed methane: A review. *Int. J. Coal Geol.* **2012**, *101*, 36–81. [CrossRef]
6. Liu, X.F.; Nie, B.S. Fractal characteristics of coal samples utilizing image analysis and gas adsorption. *Fuel* **2016**, *182*, 314–322. [CrossRef]
7. Liu, S.Q.; Sang, S.X.; Wang, G.; Ma, J.S.; Wang, X.; Wang, W.F.; Du, Y.; Wang, T. FIB-SEM and X-ray CT characterization of interconnected pores in high-rank coal formed from regional metamorphism. *J. Pet. Sci. Eng.* **2017**, *148*, 21–31. [CrossRef]
8. Wang, G.C.; Ju, Y.W.; Yan, Z.F.; Li, Q.G. Pore structure characteristics of coal-bearing shale using fluid invasion methods: A case study in the Huainan—Huaibei Coalfield in China. *Mar. Pet. Geol.* **2015**, *62*, 1–13. [CrossRef]
9. Song, Y.; Jiang, B.; Shao, P.; Wu, J.H. Matrix compression and multifractal characterization for tectonically deformed coals by Hg porosimetry. *Fuel* **2018**, *211*, 661–675.
10. Golab, A.; Ward, C.R.; Permana, A.; Lennox, P.; Botha, P. High-resolution three-dimensional imaging of coal using microfocus X-ray computed tomography, with special reference to modes of mineral occurrence. *Int. J. Coal Geol.* **2013**, *113*, 97–108. [CrossRef]
11. Pan, J.N.; Zhu, H.T.; Hou, Q.L.; Wang, H.C.; Wang, S. Macromolecular and pore structures of Chinese tectonically deformed coals studied by atomic force microscopy. *Fuel* **2015**, *139*, 94–101. [CrossRef]
12. Guan, C.; Liu, S.; Li, C.; Wang, Y.; Zhao, Y. The temperature effect on the methane and CO_2 adsorption capacities of Illinois coal. *Fuel* **2018**, *211*, 241–250. [CrossRef]
13. Meng, Z.; Liu, S.; Li, G. Adsorption capacity, adsorption potential and surface free energy of different structure high rank coals. *J Pet. Sci. Eng.* **2016**, *146*, 856–865. [CrossRef]
14. Jian, K.; Fu, X.; Ding, Y.; Wang, H.; Li, T. Characteristics of pores and methane adsorption of low-rank coal in China. *J. Nat. Gas Sci. Eng.* **2015**, *27*, 207–218. [CrossRef]
15. Yi, L.C.; Yong, Q.; Tang, H. Particle size effect of pore structure of anthracite by mercury porosimetry. *Nat. GasGe-Oscience* **2015**, *26*, 1629–1639.

16. Zhang, P.; Lu, S.; Li, J. Characterization of pore size distributions of shale oil reservoirs: A case study from Dongying sag, Bohai Bay basin China. *Mar. Pet. Geol.* **2019**, *100*, 297–308. [CrossRef]
17. Cai, Y.; Li, Q.; Liu, D.; Zhou, Y.; Lv, D. Insights into matrix compressibility of coals by mercury intrusion porosimetry and N_2 adsorption. *Int. J. Coal Geol.* **2018**, *200*, 199–212. [CrossRef]
18. Gan, H.; Nandi, S.; Walker, P., Jr. Nature of the porosity in American coals. *Fuel* **1972**, *51*, 272–277. [CrossRef]
19. Clarkson, C.R.; Solano, N.; Bustin, R.M.; Bustin, A.M.M.; Chalmers, G.R.L.; He, L. Pore structure characterization of North American shale gas reservoirs using USANS/SANS, gas adsorption, and mercury intrusion. *Fuel* **2013**, *103*, 606–616. [CrossRef]
20. Friesen, W.; Ogunsola, O. Mercury porosimetry of upgraded western Canadian coals. *Fuel* **1995**, *74*, 604–609. [CrossRef]
21. Day, S.; Fry, R.; Sakurovs, R. Swelling of Australian coals in supercritical CO_2. *Int. J. Coal Geol.* **2008**, *74*, 41–52. [CrossRef]
22. Friesen, W.I.; Mikula, R.J. Mercury porosimetry of coals: Pore volume distribution and compressibility. *Fuel* **1988**, *67*, 1516–1520. [CrossRef]
23. Friesen, W.I.; Mikula, R.J. Fractal dimensions of coal particles. *J. Colloid Interface Sci.* **1987**, *120*, 263–271. [CrossRef]
24. Harpalani, S.; Schraufnagel, R.A. Shrinkage of coal matrix with release of gas and its impact on permeability of coal. *Fuel* **1990**, *69*, 551–556. [CrossRef]
25. Spitzer, Z. Mercury porosimetry and its application to the analysis of coal pore structure. *Powder Technol.* **1981**, *29*, 177–186. [CrossRef]
26. Ritter, H.L.; Dake, L.C. Pressure porosimeter and determination of complete Macropore-Size distributions. *Ind. Eng. Chem. Anal. Ed.* **1945**, *17*, 782–786. [CrossRef]
27. Toda, Y.; Toyoda, S. Application of mercury porosimetry to coal. *Fuel* **1972**, *51*, 199–201. [CrossRef]
28. Dickinson, J.M.; Shore, J.W. Observations concerning the determination of porosities in graphites. *Carbon* **1968**, *6*, 937–941. [CrossRef]
29. Debelak, K.A.; Schrodt, J.T. Comparison of pore structure in Kentucky coals by mercury penetration and carbon dioxide adsorption. *Fuel* **1979**, *58*, 732–736. [CrossRef]
30. Jin, Y.; Zhao, M.; Liu, S.; Liu, X. Study on the effect of coal matrix compression on fractal characteristics of pore structure by mercury intrusion method. *China Coal* **2018**, *43*, 103–109.
31. Liu, J.; Ren, B.; Wang, C. Study on coal full pore aperture distribution chaeacteristics considering coal matrix compression effect. *Ind. Mine Autom.* **2022**, *48*, 125–130.
32. Han, B.B.; Qin, Y.; Zhang, Z.; Wang, G.; Yu, P. Study on coal compressibility and correction of compression amount based on compressibility of mercury injection test. *Coal Sci. Technol.* **2015**, *43*, 68–72.
33. Zheng, S.; Yao, Y.; Zhang, S.; Liu, Y.; Yang, J. Insights into Multifractal Characterization of Coals by Mercury Intrusion Porosimetry. *Energies* **2019**, *12*, 4743. [CrossRef]
34. Guo, X.Q.; Yao, Y.B.; Liu, D.M. Characteristics of coal matrix compressibility: An investigation by mercury intrusion porosimetry. *Energy Fuels* **2014**, *28*, 3673–3678. [CrossRef]
35. Ettinger, I.L.; Zhupakhina, E.S. Method of determining porosity of mineral coals. *Fuel* **1960**, *39*, 387–392.
36. Lu, J.L. Characterization of Pore Structure and Full Aperture Splicing of Coal with Different Coal Ranks. Ph.D. Thesis, China University of Mining and Technology, Xuzhou, China, 2021.
37. Cheng, L.; Li, W. Tectonic coal matrix compression characteristics based on mercury intrusion method and its impact on pore structure. *Saf. Coal Mines* **2016**, *47*, 175–179.
38. Shao, P.; Wang, X.; Song, Y.; Li, Y. Study on the characteristics of matrix compressibility and its influence factors for different rank coals. *J. Nat. Gas Sci. Eng.* **2018**, *56*, 93–106. [CrossRef]
39. Yang, Q.L.; Xue, J.H.; Li, W.; Du, X.; Ma, Q.; Zhan, K.; Chen, Z. Comprehensive evaluation and interpretation of mercury intrusion porosimetry data of coals based on fractal theory, Tait equation and matrix compressibility. *Fuel* **2021**, *298*, 120823. [CrossRef]
40. Yang, Q.L.; Li, W.; Jin, K. Supercritical CO_2 interaction induced pore morphology alterations of various ranked coals: A comparative analysis using corrected mercury intrusion porosimetry and low-pressure N_2 gas adsorption. *ACS Omega* **2020**, *5*, 9276–9290. [CrossRef]
41. Zhang, J.J.; Wei, C.T.; Zhao, J.L.; Ju, W.; Chen, Y.; Tamehe, L.S. Comparative evaluation of the compressibility of middle and high rank coals by different experimental methods. *Fuel* **2019**, *245*, 39–51. [CrossRef]
42. Zhang, B.; Zhu, J.; He, F.; Jiang, Y. Compressibility and fractal dimension analysis in the bituminous coal specimens. *AIP Adv.* **2018**, *8*, 075118. [CrossRef]
43. Li, W.; Liu, H.F.; Song, X.X. Multifractal analysis of Hg pore size distributions of tectonically deformed coals. *Int. J. Coal Geol.* **2015**, *144*, 138–152. [CrossRef]
44. Yang, Y.; Li, M.; Zhang, H.; Mi, Z.; Peng, C.; Wang, N.; Chan, Y. Evaluation of control factors and favourable zones for coalbed methane enrichment and high production in the mid-deep southern Qinshui Basin. *Nat. Gas Geosci.* **2024**, *8*, 1–12.
45. Ren, J.; Zhang, Z.; Xing, L.; Wang, P.; Yu, W.; Long, P. The Influence of Coal Body Structure on Coal Fines' Output Characteristics in the Southern Qinshui Basin. *Processes* **2024**, *12*, 656. [CrossRef]
46. Jiang, L.; Song, Y.; Zhao, W.; Bo, D.; Liu, S.; Hao, J. Main controlling factor of coalbed methane enrichment area in southern Qinshui Basin, China. *J. Pet. Explor. Prod. Technol.* **2024**, *14*, 165–173. [CrossRef]

47. Liu, J.; Chang, S.; Zhang, S.; Li, Y.; Hao, Y.; He, G.; He, Y.; Liu, B. Prediction of coalbed methane content based on seismic identification of key geological parameters: A case in a study area, Southern Qinshui Basin. *Acta Geophys.* **2023**, *71*, 2645–2662. [CrossRef]
48. Yang, C.; Qiu, F.; Xiao, F.; Chen, S.; Fang, Y. CBM Gas Content Prediction Model Based on the Ensemble Tree Algorithm with Bayesian Hyper-Parameter Optimization Method: A Case Study of Zhengzhuang Block, Southern Qinshui Basin, North China. *Processes* **2023**, *11*, 527. [CrossRef]
49. Wang, H.; Yao, Y.; Li, Z.; Yang, Y.; Yi, J.; Qiu, Y.; Zhou, S. Multi-stage gas diffusion and its implications for the productivity of coalbed methane in the southern Qinshui Basin, north China. *Front. Earth Sci.* **2023**, *17*, 109–120. [CrossRef]
50. Han, W.; Li, Y.; Wang, Y.; Ni, X.; Wang, L.; Zhou, Y. Characterization of Coal Fines and their Production Controlling Factors: A Case Study from Southern Qinshui Basin, China. *Nat. Resour. Res.* **2023**, *32*, 1777–1794. [CrossRef]
51. *SY/T 5346-2005*; Rock Capillary Pressure Measurement. Petroleum Industry Press: Beijing, China, 2005.
52. Gao, Y.; Cao, J.; Zhang, S.; Li, Z. Analysis of the Pore Structure and Fractal Characteristics of Coal and Gas Outburst Coal Seams Based on Matrix Compression Correction. *Sustainability* **2023**, *15*, 12670. [CrossRef]
53. Liu, D.; Jia, Q.; Cai, Y.; Gao, C.; Qiu, F.; Zhao, Z.; Chen, S. A new insight into coalbed methane occurrence and accumulation in the Qinshui Basin, China. *Gondwana Res.* **2022**, *111*, 280–297. [CrossRef]
54. Pape, H.; Tillich, J.E.; Holz, M. Pore geometry of sandstone derived from pulsed field gradient NMR. *J. Appl. Geophys.* **2006**, *58*, 232–252. [CrossRef]
55. Jin, Y.; Zhu, Y.B.; Li, X.; Zheng, J.L.; Dong, J.B. Scaling Invariant Effects on the Permeability of Fractal Porous Media. *Transp. Porous Media* **2015**, *109*, 433–453. [CrossRef]
56. Li, Y.; Song, D.; Liu, S.; Ji, X.; Hao, H. Evaluation of pore properties in coal through compressibility correction based on mercury intrusion porosimetry: A practical approach. *Fuel* **2021**, *291*, 0016–2361. [CrossRef]
57. Zhang, B.; Liu, W.; Liu, X. Scale-dependent nature of the surface fractal dimension for bi- and multi-disperse porous solids by mercury porosimetry. *Appl. Surf. Sci.* **2006**, *253*, 1349–1355. [CrossRef]
58. Yao, Y.B.; Liu, D.M.; Tang, D.Z.; Tang, S.H.; Huang, W.H.; Liu, Z.H.; Che, Y. Fractal characterization of seepage-pores of coals from China: An investigation on permeability of coals. *Comput. Geosci.* **2009**, *35*, 1159–1166. [CrossRef]
59. Menger, K. *Dimensionstheorie*; Vieweg+ Teubner Verlag Publishers: Wiesbaden, Germany, 1928; 324p.